The EMBO Journal vol.5 no.9 pp.2079–2085, 1986

Location of the 100 kd–50 kd accessory proteins in clathrin coats

G.P.A.Vigers[1], R.A.Crowther and B.M.F.Pearse

Medical Research Council, Laboratory of Molecular Biology, Hills Road, Cambridge CB2 2QH, UK

[1]Present address: Department of Molecular, Cellular and Developmental Biology, University of Colorado, Boulder, CO 80309, USA

Communicated by B.M.F.Pearse

We present a three-dimensional map of the clathrin coat of coated vesicles, generated from tilt series of electron micrographs of unstained specimens embedded in vitreous ice. We have examined native placental coated vesicles and coats reassembled from their purified constituents, namely clathrin triskelions and accessory proteins of approximate mol. wts 100 kd and 50 kd. Our results show that the accessory proteins contribute a further shell of density within the double shell of the clathrin cage, extending from the terminal domains of the clathrin to the membrane of the vesicle. The thickness of the complete coat is ~22 nm.

Key words: clathrin coats/frozen hydrated specimens/image reconstruction

Introduction

Clathrin-coated vesicles pinch off from certain cellular membranes, mediating the transfer of selected receptors and their ligands between cellular compartments (Goldstein *et al.*, 1979, 1985; Pearse and Bretscher, 1981). The coated membrane appears to exclude those proteins resident in the parent membrane and thus can act as a molecular filter (Bretscher *et al.*, 1980). The coat consists of clathrin and a set of 100 kd–50 kd accessory proteins (Zaremba and Keen, 1983; Pearse and Robinson, 1984). The assembly unit of clathrin is the triskelion, which has three kinked legs extending symmetrically from a vertex, each ending in a globular terminal domain (Ungewickell and Branton, 1981). We use the term 'cage' to denote a polyhedral structure of clathrin heavy chains (with or without their associated light chains) and the term 'coat' to denote a clathrin assembly which also contains 100 kd and 50 kd accessory proteins. Coats and cages may be reassembled under appropriate conditions from their purified constituents (Ungewickell and Branton, 1981; Crowther and Pearse, 1981; Zaremba and Keen, 1983; Pearse and Robinson, 1984).

We have previously reported the successful generation of three-dimensional maps from unstained frozen hydrated specimens of clathrin cages (Vigers *et al.*, 1986). These maps showed that the terminal domains of the clathrin heavy chains (Schmid *et al.*, 1982; Ungewickell *et al.*, 1982; Kirchhausen and Harrison, 1984) project inwards as fingers of density under the vertices of the outer polyhedral lattice to form an inner shell of density. We now report the results of similar studies on reconstituted coats and purified coated vesicles which reveal that the 100 kd and 50 kd accessory proteins form a further shell of density within the shell of terminal domains.

Results

We have examined two types of clathrin coats in this study: (i) native coats from preparations of coated vesicles isolated from human placenta and (ii) coats reassembled from clathrin heavy

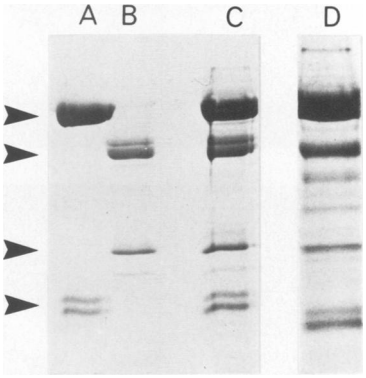

Fig. 1. Analysis of samples by SDS–polyacrylamide gel electrophoresis. **(A)** Native cages reassembled from purified bovine brain heavy and light chains. **(B)** Purified 100 kd and 50 kd accessory proteins from bovine brain. **(C)** Coats reassembled from clathrin in the presence of an excess of accessory proteins. **(D)** Native placental coated vesicles from human placenta. The positions of the heavy chains, the accessory proteins and the clathrin light chains are marked by arrows.

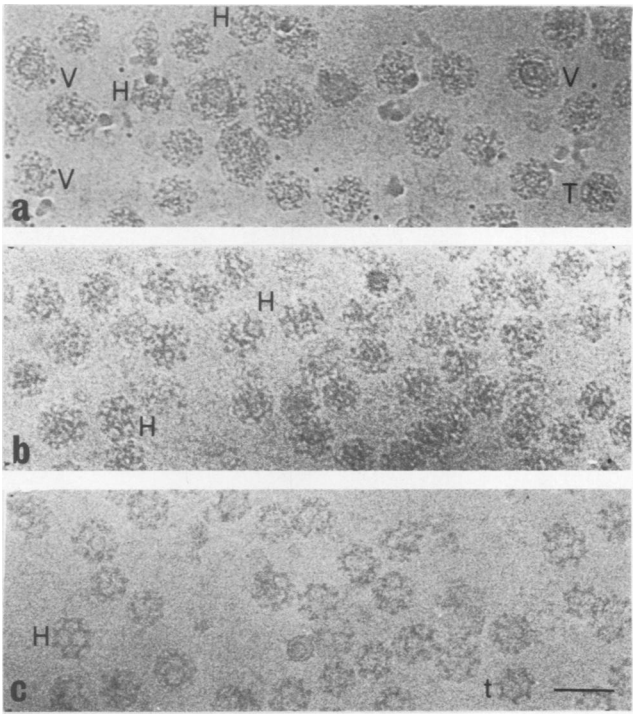

Fig. 2. Electron micrographs of unstained frozen hydrated samples. **(a)** Preparation of placental coated vesicles. **(b)** Reassembled coats. **(c)** Reassembled cages. Examples of particular types of small structures (Crowther *et al.*, 1976) are marked, namely hexagonal barrels (H), tennis balls (T) and tetrahedral particles (t). Coated vesicles (V) are also indicated. Scale bar 100 nm.

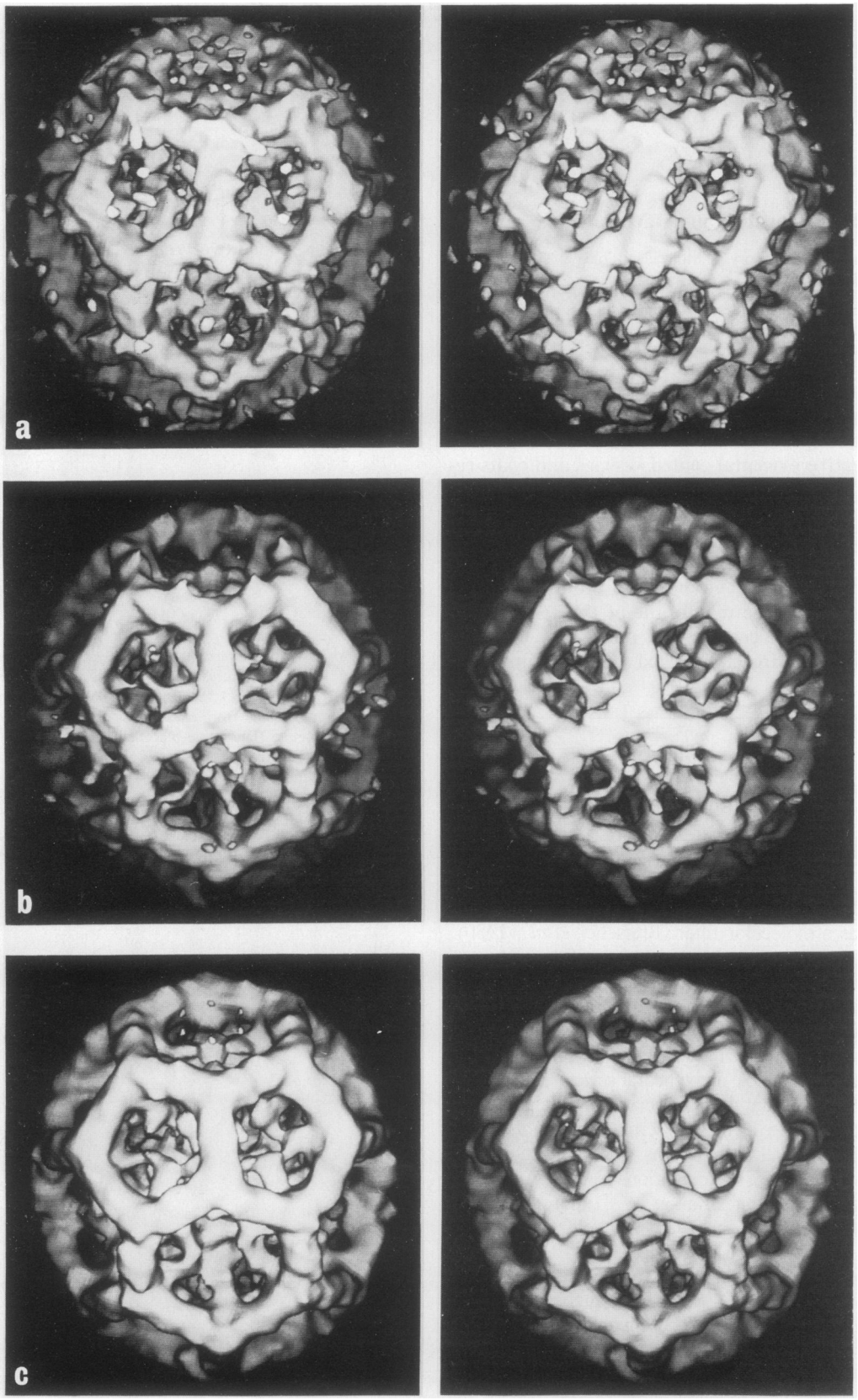

Fig. 3. Three-dimensional maps of various coat reconstructions presented as stereo-pairs. **(a)** Map from two hexagonal barrels in a preparation of placental coated vesicles. **(b)** Map from three coats reassembled from clathrin and accessory proteins. **(c)** Map from all five reconstructions added together. The noise level of this map is lower than that in **(a)** or **(b)** and the mean positions of the high density regions in the structure are now more clearly visible.

and light chains and 100 kd−50 kd proteins, which were purified from bovine brain. The biochemical constituents of the structures analysed are shown in the SDS−polyacrylamide gels reproduced in Figure 1. In coats reassembled from purified proteins there appear to be up to three molecules of the 100 kd polypeptides per clathrin triskelion, as estimated previously (Pearse and Robinson, 1984). However, in the placental preparations there are ~2 copies of 100 kd polypeptides per clathrin triskelion. In both the reassembled coats and the coated vesicles the ratio of 100 kd polypeptides to 50 kd polypeptides, though rather variable, appears to be ~2:1.

The general appearance of the specimens, when imaged unstained in vitreous ice, is shown in Figure 2. A field of native placental coated vesicles is shown in Figure 2a and a sample of reassembled bovine brain coats is shown in Figure 2b, together with a similar field of reassembled cages (without accessory proteins) in Figure 2c. Although no clear differences can be seen between individual images of the reassembled coats and cages, the coats seem to be 'fuzzier' than the cages and appear to have a dense region within them. The nature of this dense region becomes apparent after the three-dimensional reconstruction and averaging of single particles. As before we chose particles with the 'hexagonal barrel' geometry from which to make reconstructions. The hexagonal barrel has a hexagon at the top and the bottom, a ring of six hexagons around the equator and two rings each of six pentagons joining the equatorial and polar hexagons. The barrel has 622 symmetry (Crowther *et al.*, 1976) and 622 averaging was imposed on all the maps shown here. Tilt series were collected from selected areas of the specimens over a range of ±30°, and suitably aligned particles were chosen from the tilt series and processed as before (Vigers *et al.*, 1986).

Figure 3a shows a map made from two tilt series of particles in a preparation of native placental coated vesicles (Figure 2a). The reconstructions were 622 averaged and scaled (as described in Materials and methods) before they were added together. The map shows the familiar outer lattice of the hexagonal barrel, but closer examination reveals that it contains considerably more material within the outer polyhedral lattice than do the reconstructions previously calculated of cages composed only of clathrin heavy and light chains (cf. Figure 8b). This additional material appears to form a third shell of density beneath the fingers of the cage. Since the reconstructions show no evidence of a membrane vesicle within the coat, and since no vesicle could be seen in any of the small coats in the preparation of native placental coated vesicles (see below), it seems likely that the third shell of density seen in the map of the reconstructed coats is due to the presence of the 100 kd−50 kd accessory proteins. However, the placental preparation was not well characterised biochemically, so it was necessary also to make maps of coats reassembled from purified clathrin heavy and light chains in an excess of 100 kd−50 kd accessory proteins. Figure 3b shows a stereo pair of such a three-dimensional map, calculated from three independent reconstructions of reassembled coats which were scaled and added as in Figure 3a. The two maps appear very similar within the limitations imposed by the noise level of the reconstructions and in particular both contain the core of density ascribed to the accessory proteins. To improve the signal-to-noise ratio of the maps, all five three-dimensional reconstructions were added together, giving the map shown in Figure 3c. This map is less noisy than those in Figure 3a or b, and the mean positions of the constituents of the coat are now better defined. In particular, the shell of density beneath the fingers of the clathrin heavy chains and the outer polyhedral lattice is clearly visible.

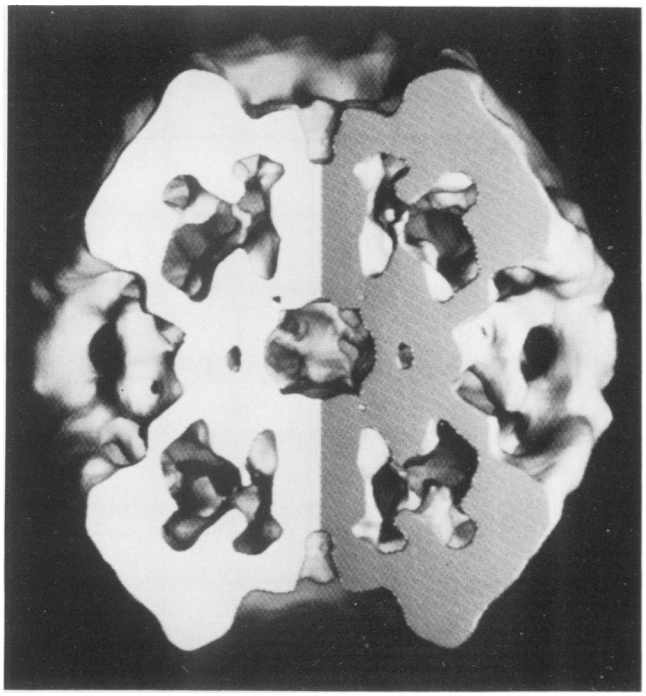

Fig. 4. The map shown in Figure 3c, viewed approximately normal to one of the equatorial hexagons but with a segment cut away to reveal the internal structure of the coat.

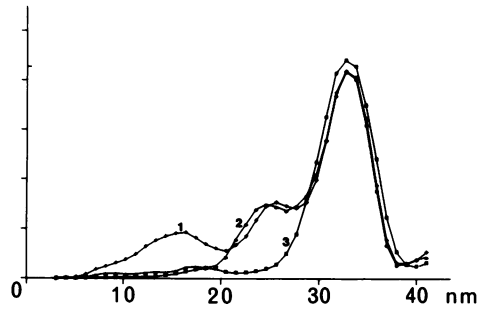

Fig. 5. Radial density functions calculated from various three-dimensional maps (Materials and methods). **Curve 1** comes from the coat map shown in Figures 3c and 4, whereas **curves 2** and **3** come respectively from maps of intact and trypsinised cages (Vigers *et al.*, 1986), which are reproduced here in Figures 8b,a. The curves demonstrate that the structures are built up as a series of shells. The strong outer peak corresponds to the outer polyhedral lattice, the middle peak to the terminal domains of the clathrin heavy chains and the inner peak to the accessory proteins.

The nature of the three shells of density in the coat structure is revealed more clearly in Figure 4, where one-third of the reconstructed particle has been cut away. The surfaces of the cut pass through the outer lattice, through eight of the heavy chain fingers and through the central core of the coat. This view shows that the core is hollow and appears to be connected to the outer lattice mainly under the equatorial and polar hexagons of the lattice. The fingers under the pentagonal faces of the outer lattice do not appear to contact the core (at least in this highly averaged map), but simply remain in the same positions that they take up in the cage. In reconstructions with less averaging, the core appears as a number of 'tubes' of high density which are continuous with the fingers of the cage (data not shown), but in other respects the less-averaged maps are difficult to interpret, due to the high noise level of the individual reconstructions.

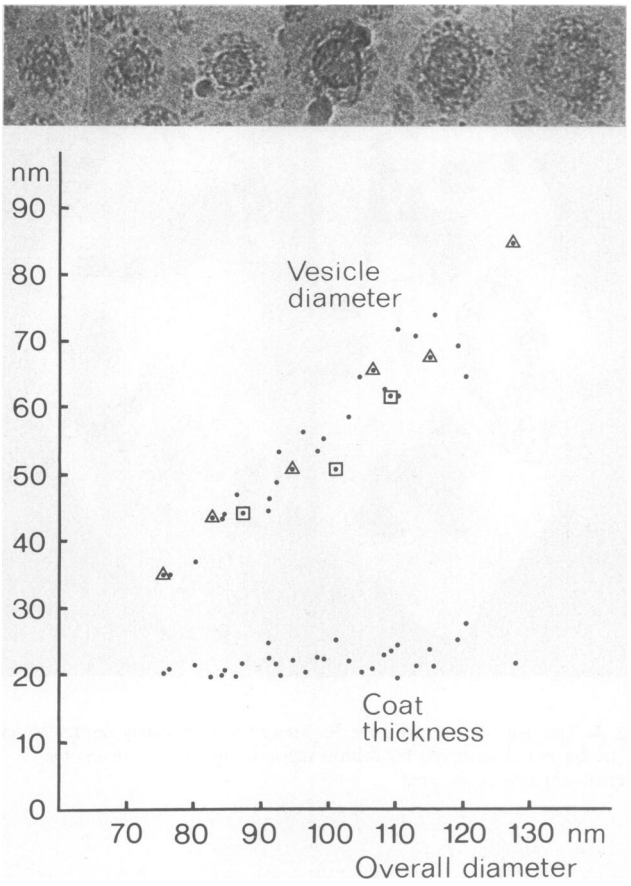

Fig. 6. Coated vesicle dimensions, showing that the coat thickness is constant irrespective of vesicle size. The mean vesicle diameter and the coat thickness are plotted against mean overall coat diameter for 30 coated vesicles from a preparation of native placental coated vesicles (part of the field is shown in Figure 2a). Six coated vesicles that span the size range (denoted by triangles) are shown in order of size above the graph. The three squares denote particles used to calculate the radial density functions shown in Figure 7a–c.

The shell-like nature of the clathrin coat is also demonstrated by the radial density functions (Figure 5) calculated from the three-dimensional maps of three types of particles (see Materials and methods). These density functions show three separate regions of the coat, which arise from the outer polyhedral lattice, the terminal domains of the heavy chains and the core of accessory proteins.

Coated vesicles in projection

Frozen-hydrated samples of native placental preparations (Figures 2a and 6) show that coated vesicles occur in a wide variety of sizes and that all but the smallest coats may contain vesicles. The vesicle viewed in projection appears as a dark disc bounded by a sharp ring of higher density. The high density of the vesicle implies that a large amount of protein must be associated with the membrane, since a bilayer of pure lipid would have a density lower than the surrounding protein. The dimensions of 30 coated vesicles are displayed in Figure 6, together with micrographs of six representative particles that span the size range found in the sample. Note that the vesicle diameter increases linearly with overall diameter of the particle, whereas the coat thickness (measured from the outside of the vesicle to the outside of the coat) remains constant at ~ 22 ± 2 nm. All coats that clearly

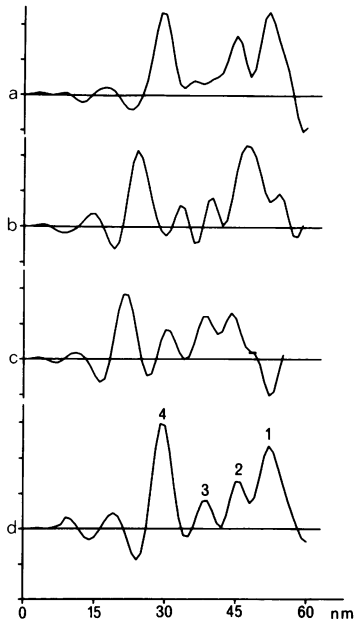

Fig. 7. Radial density functions of coated vesicles. **(a–c)** Radial density functions of three coated vesicles of successively decreasing diameter, calculated from single projected views (see Materials and methods). Each curve shows a sharp inner peak corresponding to the vesicle. **(d)** Average radial density function calculated from the three images after shifting the strong inner peak to constant radius.

contained a vesicle were found to have an outer diameter > 75 nm. Thus the minimum diameter for the vesicle in a coated vesicle in this placental preparation appears to be ~30 nm, which is approaching the lower size limit of lipid vesicles that one can make *in vitro* (Huang, 1969). The equatorial diameter of the cavity within a hexagonal barrel coat would be only ~22 nm, assuming a coat thickness of 22 nm.

Although we cannot yet make three-dimensional maps of individual coated vesicles, it is possible to calculate radial density functions from single projections of them. This calculation assumes that the coated vesicles are spherically symmetric (see Materials and methods), which is a reasonable approximation for the larger ones. Radial density functions for three selected coated vesicles of different size are shown in Figure 7a–c. Although the weights of corresponding peaks in the different functions are variable, their separations remain approximately constant, as one would expect for a coat of constant thickness surrounding a vesicle of variable radius. Figure 7d shows the average radial density function, computed from the three particles after shifting the strong inner peak (peak 4) to constant radius. Peaks 1–3 of curve d correspond respectively to the positions of the outer polyhedral lattice, the terminal domains of the clathrin heavy chains and the accessory proteins of the coat, as already shown for small coats in Figure 5. The total width of the three peaks is compressed from ~25 nm (Figure 5) to ~22 nm (Figure 7d). The strong sharp peak 4 corresponds to the vesicle itself and is the largest peak in the curve, indicating a high protein concentration. The vesicle can be seen clearly in micrographs of individual coated vesicles, as shown in Figure 6. The further peaks at smaller radius may represent the contents of the coated vesicles; but they might also be caused by phase-contrast ripples from the strong fourth peak. A three-dimensional reconstruction would be required to settle this point.

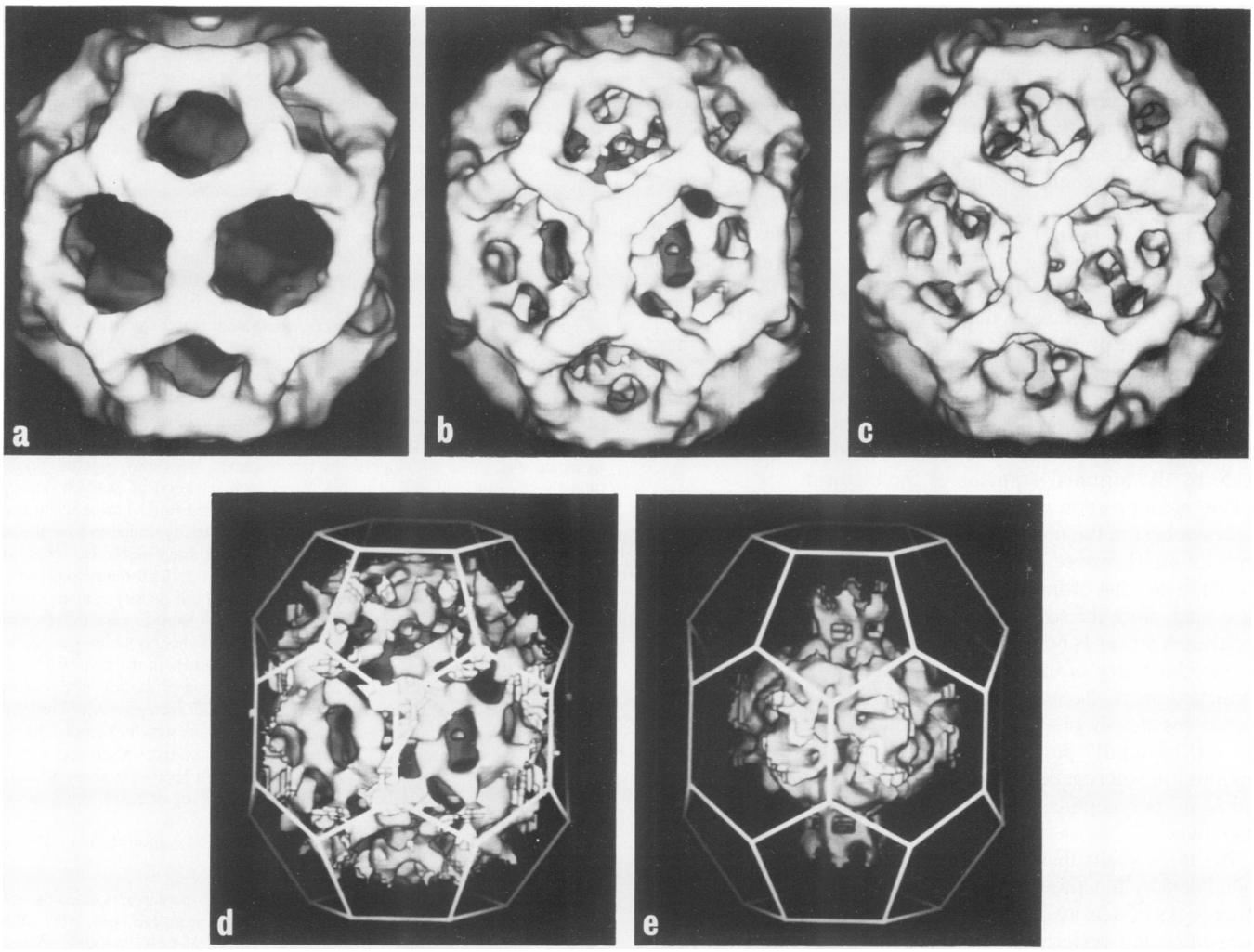

Fig. 8. Summary of various reconstructions. **(a)** Trypsinised cage and **(b)** native cage (Vigers *et al.*, 1986). **(c)** Coat as shown in Figure 3c. **(d)** Difference map calculated between the maps of the intact cage and the trypsinised cage, showing the shell of fingers corresponding to the terminal domains of the clathrin. The relationship of the fingers to the outer polyhedron is shown by the superimposed lattice. **(e)** Difference map between the coat and cage maps, showing the core of accessory proteins. The core has the shape of an oblate spheroid and appears to make contact with the fingers projecting under the polar and equatorial hexagons of the outer lattice.

Discussion

We have used electron microscopy of frozen hydrated specimens to investigate the structure of clathrin cages (which contain clathrin alone) and coats (which contain clathrin plus a set of 100 kd–50 kd accessory proteins). The technique has the advantage of preserving the specimen in a hydrated state and allows internal details of the structure to be visualised (Dubochet *et al.*, 1985). By taking a tilt series of a given area sufficient data can be collected to make three-dimensional maps of individual particles of the hexagonal barrel type. In a previous paper (Vigers *et al.*, 1986) we showed maps of clathrin cages before and after trypsin treatment, which allowed us to identify the terminal domains of the clathrin heavy chains. Here we present a three-dimensional map of the clathrin coat, which reveals for the first time the location in the coat of the 100 kd–50 kd accessory proteins. Radial density functions computed from large coated vesicles show clearly the position of the vesicle. Our results indicate that the coated vesicle is built from a series of nested shells of density, in which each shell corresponds to a biochemically defined and functionally distinct portion of the assembly.

We reproduce here (Figure 8b,a) the maps of clathrin cages before and after limited proteolysis with trypsin, to facilitate comparison with the new results on clathrin coats and to enable the overall architecture of the coat to be appreciated. In the intact cage (Figure 8b) three 'fingers' of density project from below each vertex of the outer polyhedral lattice, into the central lumen and under the three facets surrounding each vertex of the outer lattice. Limited digestion with trypsin removes the inner projections (Figure 8a), which indicates that this material corresponds to the terminal domains of the clathrin heavy chains. Thus, clathrin itself forms the outermost two shells of the coat structure and contributes both the external polyhedral lattice and the shell of fingers beneath the vertices of the cage. Our new results show that the 100 kd–50 kd accessory proteins form a third hollow shell of density below the terminal domains of the clathrin heavy chains (Figure 8c).

Surprisingly, the structure of the outer lattice and of the fingers seen in the coat appear almost identical to those in the intact cage, while the additional densities attributed to the 100 kd–50 kd proteins are found to lie almost entirely below the fingers within the cage. The shell-like organization of the material is demon-

strated clearly by the difference maps shown in Figures 8d and e. Figure 8d represents the difference between the intact cage (Figure 8b) and the trypsin-treated cage (Figure 8a), whereas Figure 8e represents the difference between the coat (Figure 8c) and the cage (Figure 8b) (difference maps were computed as described in Materials and methods). Thus Figure 8d displays the shell of heavy chain terminal domains and Figure 8e the core of accessory proteins.

Unanue *et al.* (1981) implicated the polypeptides designated as 100 kd in the binding of clathrin triskelions to a preparation of coated vesicles previously stripped of most of their clathrin. However, clathrin lacking the terminal domains binds to these stripped vesicle preparations with the same high affinity as intact triskelions, suggesting that the terminal domains are not involved in the observed binding (Hanspal *et al.*, 1984). This latter observation is difficult to reconcile with our structural interpretation that the most obvious contact with the 100 kd–50 kd shell is made by the terminal domains of the clathrin.

The mean position and distribution of the accessory proteins is shown best in the most highly averaged map of the coat (Figures 3c, 4). However, it is not possible to make any deductions about the packing of individual accessory proteins from this averaged map, since the striking local 3-fold symmetry of the fingers under each vertex is not seen in the core (cf. Figure 4). Likewise, the stoichiometry of the accessory proteins to clathrin in the reconstructions is also unclear. In the total population of coats and coated vesicles there are between two and three polypeptides of the 100 kd family per clathrin triskelion. However, the preparations are heterogeneous in particle size and geometry and the ratios of polypeptides in particular structures are therefore unknown.

The three shells that make up the coat are emphasised in the radial density functions of cages and coats (Figure 5). The same three peaks of density appear in an average of radial density functions of coated vesicles (Figure 7). Thus the features which are seen in reconstituted coats and purified empty coats are analogous to those observed in the coats of coated vesicles. In particular the coat thickness remains constant irrespective of the size of the vesicle. The vesicle appears as a further, fourth sharp inner peak in the radial density functions of coated vesicles. Unfortunately the relative sizes of the peaks may not accurately reflect the mass of the material in the different layers as their weights are affected by the contrast transfer function of the microscope arising from the large underfocus used (Lepault and Pitt, 1984).

In summary the clathrin-coated vesicle consists of a series of nested shells. The clathrin forms a two-layered outer cage with a surface lattice of long range fibrous interactions which confer mechanical stability on the structure while allowing considerable variation in curvature. The inner shell of clathrin terminal domains makes contact with a hollow 'core' of accessory 100 kd and 50 kd proteins. A fourth shell corresponds to the internal vesicle, which contains receptors that bind directly or indirectly to the coat proteins. The extra-cellular domains of the receptors and their ligands might be expected to form further shells of density within the vesicle.

Materials and methods

Preparation of samples

Clathrin was purified and reconstituted into cages as before (Pearse and Robinson, 1984). Coat proteins were solubilised from crude pellets of Triton X-100 extracted coats in a 1 M Tris-Cl buffer (pH 7.0) and separated by gel filtration on Sepharose CL-4B. Purified clathrin was reassembled into coats with column fractions containing the family of coat proteins of 100 kd and associated 50 kd polypeptide, as previously described (Pearse and Robinson, 1984). The reassembly was performed with clathrin at a concentration of 0.08 mg/ml by overnight dialysis, at 0–4°C, against 0.1 M MES–NaOH pH 7.0, 0.2 mM EGTA, 0.5 mM $MgCl_2$, 0.02% NaN_3 and 0.1 mM phenylmethylsulphonyl fluoride (PMSF) (reconstitution buffer). Aggregated material was removed by centrifugation (20 000 *g*, 10 min) and the coats were pelleted (100 000 *g*, 1 h at 5°C). The pellet was resuspended in a small volume of reconstitution buffer.

Coated vesicles from human placenta were isolated using isotonic gradients (Pearse, 1982). SDS–polyacrylamide gel electrophoresis was carried out as described previously (Pearse and Robinson, 1984), based on the procedure of Laemmli (1970). The molar ratios of the coat proteins in the gels were estimated from the colour response of the page blue 83 stain (BDH Chemicals Ltd, Poole, UK) (Fenner *et al.*, 1975).

The electron microscopy and three-dimensional reconstruction by R-weighted back projection were performed as before (Vigers *et al.*, 1986). All reconstructions were calculated to a resolution of 1/5 nm^{-1}.

Scaling of maps

Biological objects embedded in vitreous ice are imaged largely by phase contrast (Lepault and Pitt, 1984). Since different spatial frequencies in the object are represented with different weights, the reconstructed maps may contain regions of negative density and do not give a direct representation of electron density in the object (Stewart and Vigers, 1986). Care must therefore be taken when scaling the maps together. All reconstructed maps were initially scaled to have the same mean density (zero) and standard deviation (400 arbitrary units). However, since the outer polyhedral lattice of the cage was the same in all the reconstructions, and since the maps of trypsinised cages showed high density regions confined entirely to this lattice (see Figure 8a), it seemed reasonable to scale the reconstructions together such that the mean density in the polyhedral lattice was the same for all reconstructions. In order to define which pixels in the map were part of the lattice, and hence should be used for the scaling procedure, the four maps of trypsin-treated cages were added together and 622 averaged. A reference template was then constructed by taking that set of pixels which exceeded 800 units (two standard deviations) in the averaged map of the trypsinised cages. All the reconstructions were scaled to have a mean solvent level of zero in the corners of the map and the same total density within the set of pixels defined by the reference template.

All maps in this paper are displayed with a surface contour level of 450 units.

Differences between maps

The phase contrast imaging mechanism of the electron microscope and the effects of R-weighted back projection mean that a given feature can occur with different weights in the various reconstructed maps. Thus if maps were simply subtracted from each other, features common to both maps but of different densities would dominate the difference map, whereas we wish to detect strong features present in one map but absent from the other. To achieve this, differences were taken such that the pixel density in the output map was set to zero if the pixel densities in both input maps were above a set density level, but was left at the value of the first input map if this was not so. The contour level used to display the difference map was always set at the same value as that used to calculate the difference map. Thus the output map showed the regions of high density present in the first input map but not in the second. Small disconnected regions of density were removed from the difference maps displayed here, so that the major features of the maps could be seen more clearly.

Radial density functions

As before (Vigers *et al.*, 1986) radial density functions were calculated from the three-dimensional reconstructed maps of hexagonal barrels by integrating in shells about the centre of the map. The shells were given an ellipticity of 10% in the direction of the 6-fold axis of the hexagonal barrel, because the positions of the vertices of the barrel are more closely approximated by an ellipsoid than by a sphere. The results were plotted as total density per shell against shell equatorial radius. In order to remove the negative-going phase contrast ripple from around the object, a cut-off contour level of zero was specified, below which densities were ignored during the integration.

Spherical radial density functions were estimated from two-dimensional images of particles in projection by computing the cylindrical radial density function of each image. This was then converted to a spherical radial density for the three-dimensional object by successive cylindrical and spherical zero order Fourier Bessel transforms. This procedure assumes that the particle is spherically symmetric, and does not allow one to truncate negative ripples in the map. It was therefore only used to find the radial density functions of larger coated vesicles for which three-dimensional reconstructions were not available. The procedure was checked by computing radial density functions for hexagonal barrels both from three-dimensional reconstructions including negative-going ripples and from individual projected views. The features in the two sets of curves agreed well.

Acknowledgements

We thank C.Villa for assistance with photography. G.P.A.V. held an M.R.C. Research Studentship during this work.

References

Bretscher,M.S., Thomson,J.N. and Pearse,B.M.F. (1980) *Proc. Natl. Acad. Sci. USA*, **77**, 4156–4159.
Crowther,R.A. and Pearse,B.M.F. (1981) *J. Cell Biol.*, **91**, 790–797.
Crowther,R.A., Finch,J.T. and Pearse,B.M.F. (1976) *J. Mol. Biol.*, **103**, 785–798.
Dubochet,J., Adrian,M., Lepault,J. and McDowall,A.W. (1985) *Trends Biochem. Sci.*, **10**, 143–146.
Fenner,C., Traut,R.R., Mason,D.T. and Wikman-Coffet,J. (1975) *Anal. Biochem.*, **63**, 595–602.
Goldstein,J.L., Anderson,R.G.W. and Brown,M.S. (1979) *Nature*, **279**, 679–685.
Goldstein,J.L., Brown,M.S., Anderson,R.G.W., Russell,D.W. and Schneider, W.J. (1985) *Annu. Rev. Cell Biol.*, **1**, 1–39.
Hanspal,M., Luna,E. and Branton,D. (1984) *J. Biol. Chem.*, **259**, 11075–11082.
Huang,C. (1969) *Biochemistry*, **8**, 344–352.
Kirchhausen,T. and Harrison,S.C. (1984) *J. Cell Biol.*, **99**, 1725–1734.
Laemmli,U.K. (1970) *Nature*, **227**, 680–685.
Lepault,J. and Pitt,T. (1984) *EMBO J.*, **3**, 101–105.
Pearse,B.M.F. (1982) *Proc. Natl. Acad. Sci. USA*, **79**, 451–455.
Pearse,B.M.F. and Bretscher,M.S. (1981) *Annu. Rev. Biochem.*, **50**, 81–101.
Pearse,B.M.F. and Robinson,M.S. (1984) *EMBO J.*, **3**, 1951–1957.
Schmid,S.L., Matsumoto,A.K. and Rothman,J.E. (1982) *Proc. Natl. Acad. Sci. USA*, **79**, 91–95.
Stewart,M. and Vigers,G.P.A. (1986) *Nature*, **319**, 631–636.
Unanue,E.R., Ungewickell,E. and Branton,D. (1981) *Cell*, **26**, 439–446.
Ungewickell,E. and Branton,D. (1981) *Nature*, **289**, 420–422.
Ungewickell,E., Unanue,E.R. and Branton,D. (1982) *Cold Spring Harbor Symp. Quant. Biol.*, **46**, 723–731.
Vigers,G.P.A., Crowther,R.A. and Pearse,B.M.F. (1986) *EMBO J.*, **5**, 529–534.
Zaremba,S. and Keen,J.H. (1983) *J. Cell Biol.*, **97**, 1339–1347.

Received on 2 June 1986